Human Mutation

Clinical and functional characterization of two novel *ZBTB20* mutations causing Primrose syndrome

Journal:	*Human Mutation*
Manuscript ID	Draft
Wiley - Manuscript type:	Brief Report
Date Submitted by the Author:	n/a

Complete List of Authors:	Stellacci, Emilia; Istituto Superiore di Sanità, Oncologia e Medicina Molecolare Steindl, Katharina; Institute of Medical Genetics, University of Zurich Joset, Pascal; Institute of Medical Genetics, University of Zurich Mercurio, Laura; Istituto Superiore di Sanità, Oncologia e Medicina Molecolare Anselmi, Massimiliano; Università di Roma 'Tor Vergata', Dipartimento di Scienze e Tecnologie Chimiche Cecchetti, Serena; Istituto Superiore di Sanità, Servizio grandi strumentazioni e core facilities Gogoll, Laura; Institute of Medical Genetics, University of Zurich Zweier, Markus; Institute of Medical Genetics, University of Zurich Hackenberg, Annette; University Children's Hospital Zürich, Division of Pediatric Neurology Bocchinfuso, Gianfranco; Università di Roma 'Tor Vergata', Dipartimento di Scienze e Tecnologie Chimiche Stella, Lorenzo; Universita' "Tor Vergata", Dipartimento di Scienze e Tecnologie Chimiche Tartaglia, Marco; Bambino Gesù Children’s Hospital, IRCCS, Division of Genetic Disorders and Rare Diseases Rauch, Anita; University of Zurich, Institute of Medical Genetics
Key Words:	Primrose syndrome, ZBTB20, 3q13.31 microdeletion syndrome, mutation spectrum, functional analyses

Clinical and functional characterization of two novel *ZBTB20* mutations causing Primrose syndrome

Emilia Stellacci[1]*, Katharina Steindl[2]*, Pascal Joset[2], Laura Mercurio[1], Massimiliano Anselmi[3], Serena Cecchetti[4], Laura Gogoll[2], Markus Zweier[2], Annette Hackenberg[5], Gianfranco Bocchinfuso[3], Lorenzo Stella[3], Marco Tartaglia[6§], Anita Rauch[2,7,8,9§]

[1] Dipartimento di Oncologia e Medicina Molecolare, Istituto Superiore di Sanità, Rome, Italy;
[2] Institute of Medical Genetics, University of Zurich, Schlieren-Zurich, Switzerland;
[3] Dipartimento di Scienze e Tecnologie Chimiche, Universita` di Roma ‘‘Tor Vergata’’ Rome, Italy;
[4] Servizio grandi strumentazioni e core facilities, Istituto Superiore di Sanità, Rome, Italy;
[5] Division of Paediatric Neurology, University Children’s Hospital Zurich, Zürich, Switzerland;
[6] Genetics and Rare Diseases Research Division, Ospedale Pediatrico Bambino Gesù, Rome, Italy;
[7] radiz—Rare Disease Initiative Zürich, Clinical Research Priority Program for Rare Diseases University of Zurich, Zurich, Switzerland
[8] Neuroscience Center Zurich, University of Zurich and ETH Zurich, Zurich, Switzerland
[9] Zurich Center for Integrative Human Physiology, University of Zurich, Zurich, Switzerland

*These authors equally contributed to this work.
[§]These authors jointly coordinated this work.

[*]Corresponding authors:

Emilia Stellacci,
Department of Oncology and Molecular Medicine,
Istituto Superiore di Sanità,
Viale Regina Elena, 299, Rome 00161, Italy.
Phone: +390649903197; e-mail: emilia.stellacci@iss.it

Katharina Steindl,
Institute of Medical Genetics,
University of Zurich,
Wagistrasse 12, 8952 Schlieren-Zurich, Switzerland.
Phone: +41445563300; e-mail: steindl@medgen.uzh.ch

Disclosure statement:

The authors declare no conflict of interest.

Acnowledgements

We are grateful to the families who contributed to this study. We thank Serenella Venanzi for technical support. This study was supported by grants from the University of Zurich clinical research priority program radiz (rare disease initiative Zurich), Fondazione Bambino Gesù (*Vite coraggiose*) and Fondazione Umberto Veronesi.

ABSTRACT

Primrose syndrome (PS) is a rare disorder characterized by macrocephaly, tall stature, intellectual disability, autistic traits, and disturbances of glucose metabolism with insulin-resistant diabetes and distal muscle wasting occurring in adulthood. The disorder is caused by functional dysregulation of ZBTB20, a transcriptional repressor controlling energetic metabolism and developmental programs. *ZBTB20* maps in a genomic region that is deleted in the 3q13.31 microdeletion syndrome, which explains the partial clinical overlap between the two disorders. A narrow spectrum of amino acid substitutions in a restricted region of ZBTB20 encompassing the first and second zinc-finger motifs have been reported thus far. Here, we characterize clinically and functionally the first truncating mutation (c.1024delC; p.Gln342Serfs*42) and a missense change affecting the third zinc-finger motif of the protein (c.1931C>T; p.Thr644Ile). Our data document that both mutations have dominant negative impact on wild-type ZBTB20, providing further evidence of the specific behavior of PS-causing mutations on ZBTB20 function.

Keywords: Primrose syndrome, *ZBTB20*, 3q13.31 microdeletion syndrome, mutation spectrum, functional analyses.

MAIN TEXT

Recognized as a nosologic entity for the first time over 35 years ago (Primrose, 1982), Primrose syndrome (PS; MIM #259050) is a rare genetic condition characterized by cognitive deficits often associated with autism spectrum disorder, macrocephaly, tall stature, truncal obesity, and a distinctive pattern of ectopic calcification. With age, deafness, atrophy of the muscles of the limbs, disturbed glucose metabolism and onset of diabetes in adults is commonly observed in affected individuals (Collacott et al, 1986; Lindor et al, 1996; Battisti et al, 2002; Dalal et al, 2010; Posmyk et al, 2011; Carvalho et al, 2011). The assumption of autosomal dominant inheritance of this sporadic condtion was confirmed by the identification of heterozygous *de novo* missense mutations in *ZBTB20* as the molecular event underlying the trait (Cordeddu et al, 2014). Consistent with the occurrence of intellectual disability, behavioral issues and altered energetic metabolism in PS patients, ZBTB20 is a transcriptional repressor involved in the control of brain development and glucose metabolism (Sutherland et al, 2009; Mitchelmore et al, 2002; Nielsen et al, 2007). The protein is a member of the broad complex tramtrack bric-a-brac (BTB) zinc-finger family (Zhang et al, 2001; Zhang et al, 2012; Zhang et al, 2015), and is characterized by an *N*-terminal BTB domain that is involved in protein-protein interaction, and five C2H2 zinc fingers at the *C*-terminus mediating protein binding to regulatory sites within promoters of target genes. So far, all mutations causing PS have been reported to be missense and affect amino acid residues within a region of the protein encompassing the first and second zinc-finger (ZnF) motifs (Cordeddu et al, 2014; Mattioli et al, 2016) (Figure 1A). *ZBTB20* maps in a relatively small region containing a few additional protein-coding genes (*DRD3*, *ZNF80*, and *TIGIT*) that is deleted in the 3q13.31 microdeletion syndrome (del3q13.31, MIM #615433), a complex condition clinically overlapping PS and characterized by postnatal growth in the upper normal range, hypotonia, intellectual disability (ID), developmental delay, disturbed behavior and dysmorphic features (Hervé et al, 2016). Of note, we previously provided evidence for a dominant negative impact of PS-causing mutations, indicating that PS and del3q13.31 syndrome may represent allelic disorders resulting from variably impaired

ZBTB20 function (Cordeddu et al, 2014). Here, we report on the clinical and functional characterization of two novel *ZBTB20* mutations, a truncating frameshift (c.1024delC; p.Gln342Serfs*42) and a missense substitution (c.1931C>T; p.Thr644Ile) affecting the third ZnF motif, identified by whole exome sequencing (WES) in two young individuals with ID, macrocephaly and syndromic features. We document that both changes result in stable but dysfunctional proteins characterized by impaired/defective binding to DNA, and provide further evidence for their dominant negative impact on ZBTB20 function.

The study was approved by the University Children's Hospital of Zurich, and written informed consent was obtained from each participant for DNA storage and genetic analyses. Patient 1 (P1) was an 8.5 year-old boy with mild developmental delay and macrocephaly born to non-consanguineous healthy parents from the Dominican Republic (Figure 1B upper panels and Suppl. Table 1). He was born at 35 + 3/7 weeks of gestation by Caesarean section with a weight of 2465 g (25th centile), length of 44 cm (5th centile), and head circumference of 34.8 cm (75th-90th centile).The new-born hearing assessment was reported to be normal and confirmed by formal testing at 8.5 years. Motor development was delayed with unsupported sitting at 11 months, and independent walking at 18 months. He had macrocephaly, and brain MRI at 19 months revealed prominent subarachnoid spaces, and hypoplastic corpus callosum and a small pituitary pars intermedia cyst. At 3 years the SON-R 2.5-7 test evidenced an IQ of 77 and a higher performance in analogical reasoning. At 5 years, bilingual speech development and social skills were considered within the normal limits. Sleeping apnoea was successfully treated by tonsillectomy, and orchidopexy was performed at age 6 years. Truncal ataxia, which had previously been reported when the child was 18 months, remained only minimal at the age of 6 years. At the age of 7.5 years, his height was 132 cm (90th centile), weight was 32.3 kg (97th centile), and head circumference was 59 cm (>97th centile; +4.3 SDS) with prominent occiput. He had convergent strabismus (left eye). His facial features included a narrow forehead, underdeveloped supraorbital ridges, medial flaring and laterally sparse eyebrows, narrow palpebral fissures, malar flattening, wide and depressed nasal

bridge, broad nasal tip, short and deep philtrum, thick and everted upper and lower lip vermillion, hypotonic open mouth appearance, and overfolded helices and posteriorly angulated ears with large, forward facing lobes. He had mild upper incisor diastema and delayed eruption of teeth. At age of 8.5 years, he attended a special education school due to reduced short-term memory and short attention span. He showed no obvious behavioural issue, and was described as very sensitive. Daytime urinary continence was achieved at almost 4 years, but nighttime toilet training was still not completed at 8.5 years. At the age of 9 years, ankle contractures were noticed. High-resolution chromosomal microarray testing using an Affymetrix Cytoscan HD array at a 20kb resolution showed normal results.

Patient 2 (P2) was a 3 year-old girl with global developmental delay and macrocephaly born to a healthy non-consanguineous couple of Swiss origin (Figure 1B lower panel and Suppl. Table 1). Polyhydramnios and increased head circumference were noted prenatally. Delivery took place at 41 + 3/7 weeks of gestation and required vacuum extraction. Her birthweight was 3320 g (25-50th centile), birth length 53 cm (50-75th centile) and the head circumference 37 cm (90th centile). The newborn screening test for hearing failed. Formal testing confirmed a bilateral hypoacusis, more pronounced on the right side, treated with hearing aids. A cranial MRI was performed at 10 months of age showing partial agenesis of the corpus callosum. An EEG showed no abnormalities. The patient was referred to the genetic clinic at 14 month of age for macrocephaly, developmental delay and muscular hypotonia. Her anthropometric measurements were: weight 10 kg (50-75th centile), length 79.5 cm (75-90th centile) and head circumference 50.5 cm (> 97th centile). She had a broad face and forehead, high anterior hairline, full and curly hair, long ears with increased posterior angulation, short palpebral fissures with deeply set eyes, convergent strabismus, underdeveloped supraorbital ridges, medial flaring of eyebrows with lateral thinning, malar flattening, full cheeks, prominent nasal bridge with wide nasal base, short columella, mildly thickened alae nasi, deep philtrum, thin upper lip vermillion and mildly everted lower lip vermillion, slightly downturned angles of the mouth, and a diastema of the upper central incisors. She had short hands, broadened

thumbs, short terminal phalanges of the 5th fingers bilaterally, deep palmar creases, and bilateral sandal gaps. She had hypertrichosis of the back and a café-au-lait spot on her left forearm. The girl was followed in the neurodevelopmental clinic for her global psychomotor development delay. She sat unsupported at 19 months and walked independently at 24 months. At 3 years and 4 months, her speech was still confined to a few simple words, and the mother described her as stubborn and not able to follow commands. Neurologic exam revealed muscular hypotonia of the extremities and the trunk. High-resolution chromosomal microarray testing using an Affymetrix Cytoscan HD array at a 20 kb resolution showed normal results.

WES was performed in both affected individuals (Supplemental Methods) obtaining an average depth of coverage of 282x (P1) and 196x (P2), with 97.2% and 96.1% of the targeted bases with ≥20 reads, respectively. In P1, data filtering and prioritization allowed to identify the unreported heterozygous c.1024delC (NM_001164342.2) variant within exon 4 of the *ZBTB20* gene as the best disease-causing candidate. The single base deletion was predicted to cause premature translational termination (p.Gln342Serfs*42, NP_001157814.1), resulting in a protein lacking the entire C-terminal ZnF domain and having disrupted DNA binding capacity. Sanger sequencing confirmed the variant and provided evidence for its *de novo* occurrence (Suppl. Fig. 1A). In P2, trio analysis revealed 4 putative *de novo* variants, including an unreported missense variant in exon 5 of *ZBTB20* (c.1931C>T, p.Thr644Ile), affecting a residue highly conserved among ZBTB20 orthologs and located within the third ZnF motif. The variant was predicted to be deleterious (CADD score: 29.2), and was confirmed in the patient and excluded in the parents by Sanger sequencing, demonstrating its *de novo* origin (Suppl. Fig. 1B). In this subject, three additional *de novo* variants were identified as *de novo* events. A previously unreported missense change (c.1927G>A [NM_002047.2], p.Val643Ile [NP_002038.2]) in *GARS* was not considered causative for the trait because of the relatively poor predicted impact (CADD score: 14.5) and based on the consideration that mutations in this gene cause distal hereditary motor neuronopathy (MIM #600287) and Charcot-Marie-Tooth disease type 2D (MIM #601472). . Similarly, the private intronic variant

c.2573-5G>A in *JAG1* (NM_000214.2) did not fulfill criteria for pathogenicity because *in silico* predictions did not indicate a relevant impact on transcript processing. Finally, the missense change c.1288G>A (NM_001258428.1; p.Ala454Thr, NP_001245357.1) in *SLC4A9* was reported once in the ExAC database (rs766993747) and did not have any available evidence for pathogenicity (CADD score: 0.20) and clinical relevance, being SLC4A9 a member of the Slc4a family of Cl(-)/HCO3 (-) exchangers and Na(+)-HCO3 (-) cotransporters. In both subjects, no gene with biallelic private/rare variants with predicted functional impact was retained after filtering. DNA from saliva was available for the two probands, and genotyping confirmed the presence of the mutations in both, providing evidence for the likely germline origin of both mutations.

We previously generated a model of the ZnF region of ZBTB20 complexed with DNA to explore the structural and functional impact of the PS-causing amino acid substitutions on DNA binding properties of the domain (Cordeddu et al, 2014). By using this model, we inspected the impact of the Thr644Ile amino acid substitution, and observed that Thr644 directly participates in non-specific interactions with DNA, forming a hydrogen bond with the phosphate group of the DNA backbone (Fig. 1C, upper box). Its substitution by the branched, non-polar isoleucine residue removes the H-bond, possibly causing also unfavorable interactions with both nearby residues and DNA, affecting protein-DNA interaction (Fig. 1C, bottom box).

To assess further the functional relevance of the novel *ZBTB20* variants, we performed biochemical studies in transiently transfected HEK293 cells. Western blot analysis documented that both the Xpress-tagged ZBTB20 mutants were efficiently expressed, and that they were more stable compared to the wild-type protein (Fig. 2A). This finding, which was unexpected for truncating mutantion, is in line with the collected data for a panel of PS-causing *ZBTB20* mutants (Cordeddu et al, 2014). Similarly to what was previously observed for the other *ZBTB20* mutants, confocal microscopy analysis documented the nuclear localization of the two mutants. Differently from wild type ZBTB20, however, both proteins showed a non-homogeneous distribution pattern (Fig. 2B upper panels). Moreover, as observed by treatment with cytoskeleton (CSK) buffer, which allows

removal of nuclear proteins weakly bound to chromatin, both mutants appeared to not stably bind to chromatin, differently from what observed for the wild-type protein (Fig. 2B lower panels). Of note, co-expression of FLAG-tagged wild-type ZBTB20 with each of the Xpress-tagged mutants showed co-localization of wild-type and mutant ZBTB20 proteins in untreated cells (Fig. 2C, upper panels) and a significant reduction of the wild-type protein after CSK treatment, indicating a dominant impact of the two mutants, probably mediated by heterodimerization (Fig. 2C, lower panels). To further confirm the impaired/defective interaction of mutants with DNA, DNA binding assays were performed in transiently transfected HEK293 cells using biotinylated oligos encompassing the *AFP* promoter minimal responsive sequence (Zhang et al, 2015). A strongly reduced DNA binding of the Thr644Ile mutant and, as expected, complete absence of binding of the p.Gln342fs*42 truncated ZBTB20 protein were observed (Fig. 2D, lane 3 and 5 left panel). Consistent with the previously collected data, cells co-expressing wild-type ZBTB20 and each of the two disease-causing mutants showed a less efficient binding to the *AFP* promoter (Fig. 2D, lane 2 and 4 left panel), providing additional evidence for the dominant negative impact of both mutations.

PS is a rare and multisystem disorder whose prevalence is possibly underestimated. So far, a bunch of missense heterozygous mutations affecting the first two ZnF motifs of the protein have been described. Here, we report on two novel germline mutations in young patients resembling PS. While both mutations affected the functional domain of the repressor mediating DNA binding, one of the two variants, c.1024delC, substantially differed from the previously reported disease-causing *ZBTB20* mutations (Cordeddu et al, 2014) since it is truncating and is predicted to result in a protein lacking the entire region mediating binding to DNA. Similarly, the second pathogenic variant, c.1931C>T, affects a residue located within the third ZnF motif of the protein, a portion of the DNA-binding domain that was not previously reported to be affected. Functional data underlined that both mutations perturb ZBTB20's function by impairing proper binding of the repressor to DNA, with a dominant negative effect. This report also offers new information on the clinical characterization and natural history of PS, providing detailed data on this disorder during childhood.

Both affected individuals exhibited postnatal growth in the upper range, macrocephaly, hypoplasia of the corpus callosum, hypotonia, variable intellectual disability and distinctive facial features. They did not present disturbed glucose metabolism, cataracts and ectopic calcification of the ears and brain, which probably occur in PS later during puberty or early adulthood. Distal muscle wasting leading to progressive contractures was not yet evident in the young P2, but in P1 ankle contractures were noticed at age 9 years. Notably, these data suggest that both the dominant negative-acting mutations underlying PS and haploinsufficiency of ZBTB20 associated with the 3q13.31 microdeletion result in a similar clinical phenotype during childhood despite the apparent difference in pathomechanism. It should be noted that currently available description of the clinical phenotype associated with the 3q13.31 microdeletion and PS do not allow to assess accurately possible genotype-phenotype associations as well as to compare the natural history of the two disorders. Of note, muscle wasting, joint contractures and disturbed glucose metabolism were never reported in patients with the microdeletion syndrome and therefore we might expect a differential perturbing effect of the two classes of defects later during adulthood, even though a more detailed and systematic analysis of the clinical features characterizing the two disorders should be performed to verify this hypothesis.

In conclusion, our findings further strengthen the genetic link between PS and the 3q13.31 microdeletion syndrome, widen the molecular spectrum of *ZBTB20* mutations and confirm the dominant negative impact of PS-causing mutations on ZBTB20 function.

SUPPORTING INFORMATION

Additional supporting information may be found in the online version of this article at the publisher's web-site.

REFERENCES

Battisti C, Dotti MT, Cerase A, Rufa A, Sicurelli F, Scarpini C, Federico A. 2002. The Primrose syndrome with progressive neurological involvement and cerebral calcification. J Neurol 249:1466-1468.

Carvalho, D. R., Speck-Martins, C. E. 2011. Additional features of unique Primrose syndrome phenotype. Am J Med Genet 155A:1379-1383.

Collacott RA, O'Malley BP, Young ID. 1986. The syndrome of mental handicap, cataracts, muscle wasting and skeletal abnormalities: report of a second case. J Ment Defic Res 30:301-308.

Cordeddu V, Redeker B, Stellacci E, Jongejan A, Fragale A, Bradley TE, Anselmi M, Ciolfi A, Cecchetti S, Muto V, Bernardini L, Azage M, et al. 2014. Mutations in ZBTB20 cause Primrose syndrome. Nat Genet 46(8):815–817.

Dalal P, Leslie ND, Lindor NM, Gilbert DL, Espay AJ. 2010. Motor tics, stereotypies, and self-flagellation in primrose syndrome. Neurology 75(3):284–286.

Hervé B, Fauvert D, Dard R, Roume J, Cognard S, Goidin D, Lozach F, Molina-Gomes D, Vialard F. 2016. The emerging microduplication 3q13.31: Expanding the genotype-phenotype correlations of the reciprocal microdeletion 3q13.31 syndrome. Eur J Med Genet 59(9):463-469.

Lindor NM, Hoffman, AD, Primrose DA. 1996. A neuropsychiatric disorder associated with dense calcification of the external ears and distal muscle wasting: 'Primrose syndrome'. Clin Dysmorph 5:27-34.

Mattioli F, Piton, A, Gerard B, Superti-Furga A, Mandel JL, Unger S. 2016. Novel de novo mutations in ZBTB20 in Primrose syndrome with congenital hypothyroidism. Am J Med Genet 170A:1626-1629.

Mitchelmore C, Kjaerulff KM, Pedersen HC, Nielsen JV, Rasmussen TE, Fisker MF, Finsen B, Pedersen KM, Jensen NA. 2002. Characterization of two novel nuclear BTB/POZ domain zinc

finger isoforms. Association with differentiation of hippocampal neurons, cerebellar granule cells, and macroglia. J Biol Chem 277(9):7598–7609.

Nielsen JV, Nielsen FH, Ismail R, Noraberg J, Jensen NA. 2007. Hippocampus-like corticoneurogenesis induced by two isoforms of the BTB-zinc finger gene Zbtb20 in mice. Development 134:1133-1140.

Posmyk R, Lesniewicz R, Chorązy M, Wołczynski S. 2011. New case of Primrose syndrome with mild intellectual disability. Am J Med Genet Part A 155A:2838–2840.

Primrose DA. 1982. A slowly progressive degenerative condition characterized by mental deficiency, wasting of limb musculature and bone abnormalities, including ossification of the pinnae. J Ment Defic Res 26:101–106.

Sutherland AP, Zhang H, , Michaud M, Xie Z, Patti ME, Grusby MJ, Zhang WJ. 2009. Zinc finger protein Zbtb20 is essential for postnatal survival and glucose homeostasis. Mol. Cell Biol 29(10):2804-2815.

Zhang W, Mi J, Li N, Sui L, Wan T, Zhang J, Chen T, Cao X. 2001. Identification and characterization of DPZF, a novel human BTB/POZ zinc finger protein sharing homology to BCL6. Biochem Biophys Res Commun 282(4):1067–1073.

Zhang Y, Xie Z, Zhou L, Li L, Zhang H, Zhou G, Ma X, Herrera PL, Liu Z, Grusby MJ, Zhang WJ. 2012. The zinc finger protein ZBTB20 regulates transcription of fructose-1,6-bisphosphatase 1 and β cell function in mice. Gastroenterology 142:1571–80.

Zhang H, Cao D, Zhou L, Zhang Y, Guo X, Li H, Chen Y, Spear BT, Wu JW, Xie Z, Zhang WJ. 2015. ZBTB20 is a sequence-specific transcriptional repressor of alphafetoprotein gene. Sci Rep 5, 11979; doi:10.1038/srep11979.

FIGURE TITLES AND LEGENDS

Figure 1. Location of *ZBTB20* mutations causing Primrose syndrome, facial features of the two affected individuals, and homology model of the ZBTB20-DNA complex. A) ZBTB20 domain structure (BTB domain, red box; ZnFs, green boxes) and location of residues affected by the present (red) and previously reported (blue [Cordeddu et al. 2014] and green [Mattioli et al, 2016]) mutations. **B)** Facial features of P1 at the age of 5 years and 3 months (upper panel) and 7 years and 5 months (medium panel), and those of P2 at the age of 3 years and 4 months (lower panel). **C)** Homology model of the DNA-bound ZBTB20 region encompassing the ZnF motifs 1 to 4 (brown ribbon, with residues affected by previously reported mutations colored in blue or green, as in panel A). DNA backbone (gold ribbon), bases (sticks) and phosphates (dotted spheres) are also shown. Thr^{644} (reported in sticks representation) forms a hydrogen bond (shown as a green dashed line) with a phosphate group (sticks) of the DNA backbone (upper box), which is lost with substitution to Ile (lower box).

Figure 2. Impact of the two identified disease-causing mutations on ZBTB20 function. A) Levels of X-press tagged wild-type and mutant ZBTB20 proteins. Fifty micrograms of whole cell extract where analyzed by western blot using an anti-Xpress antibody. Images are representative of three experiments performed. **B)** Subcellular localization of ZBTB20 proteins. ZBTB20 mutants display nuclear localization but appear not stably bound to chromatin. Confocal microscopy analysis was performed in cells expressing wild-type ZBTB20 or the two disease-causing mutants (green), without or with treatment with CSK buffer prior fixation. Nuclei are DAPI stained (blue). Bars correspond to μm indicated in the figure. **C)** ZBTB20 proteins co-localization. X-press tagged ZBTB20 mutants co-localized with FLAG-tagged wild-type ZBTB20. A substantial reduction of ZBTB20 localizing into nuclei after CSK treatment is observed. Only 20-25% of cells maintains a nuclear double staining. Confocal microscopy analysis was performed in cells expressing wild-type

ZBTB20 (green) and the two disease-causing mutants (red), without or with treatment with CSK buffer prior fixation. Nuclei are DAPI stained (blue). Bars correspond to 10 μm. **D)** DNA binding assay performed on lysates from cells transfected with ZBTB20 constructs as indicated using biotinylated oligos covering the minimal responsive sequence of the *AFP* promoter. Reduced DNA binding is observed in extracts from cells overexpressing each of the two ZBTB20 mutants, and is also documented in extracts from cells co-expressing each mutant with the wild-type protein (left). Western blots of a representative experiment of three performed are shown.

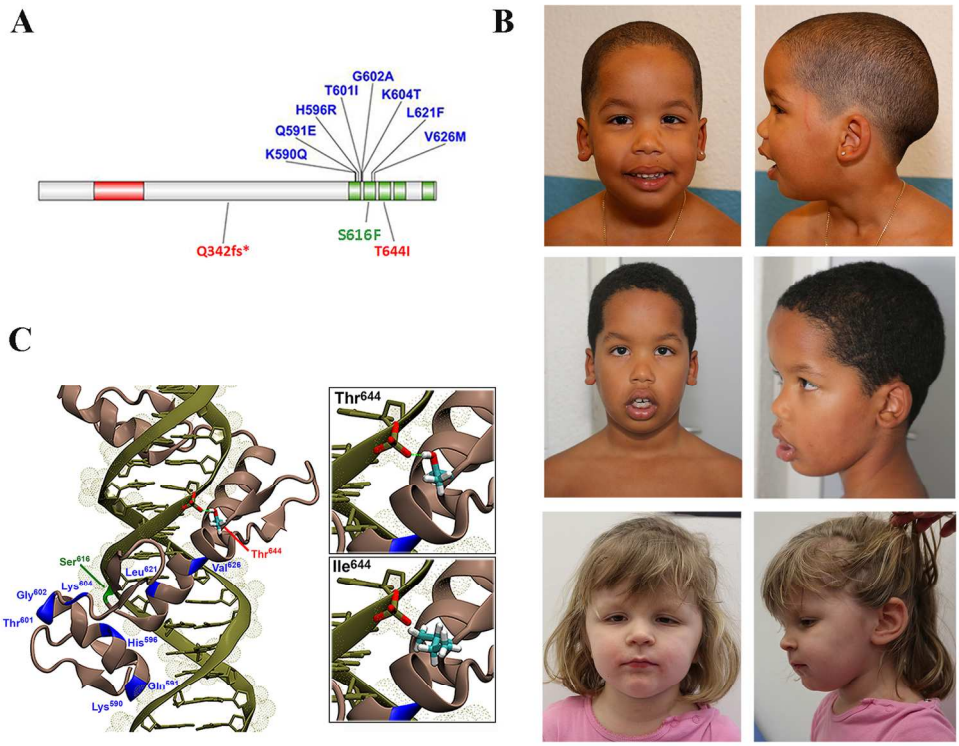

Figure 1. Location of *ZBTB20* mutations causing Primrose syndrome, facial features of the two affected individuals, and homology model of the ZBTB20-DNA complex.

150x120mm (300 x 300 DPI)

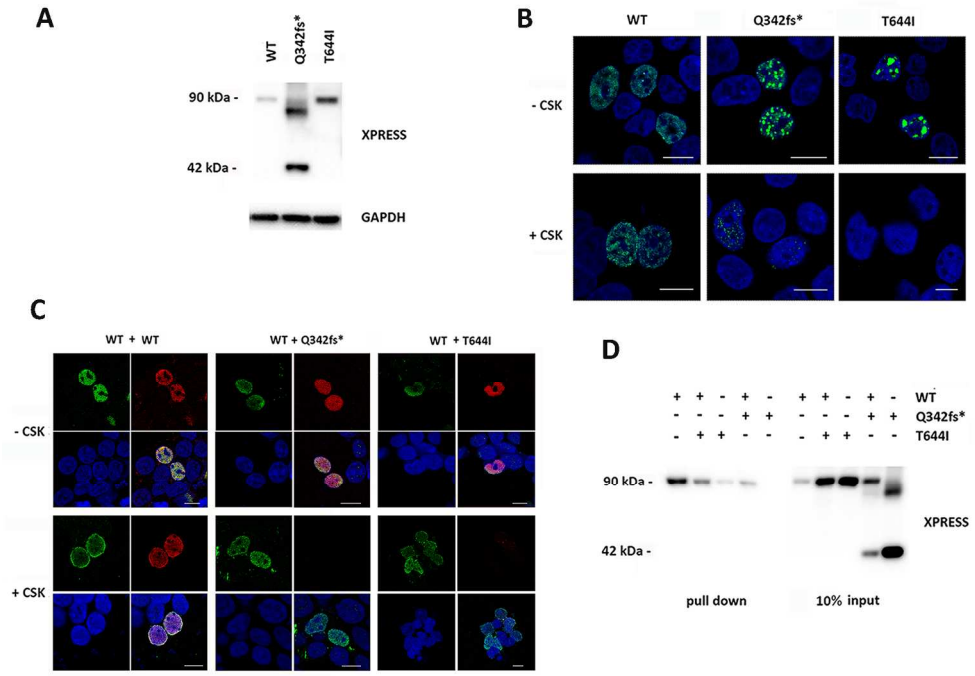

Figure 2. Impact of the two identified disease-causing mutations on ZBTB20 function.

180x128mm (300 x 300 DPI)

Supplemental Table 1. Clinical features of patients with *ZBTB20* mutations.

Individuals	P1	P2	Primrose syndrome	3q13.31 del syndrome
ZBTB20 amioacid change	Gln342Serfs*42	Thr644Ile		
Age at last investigation (years)	8.5	3.4	25.4 (mean)	9.2 (mean)
Gender	M	F	4M/4F	6M/6F
Polyhydramnios	NA	from GW 30	NA	NA
Week of gestation	35 3/7	41 3/7	NA	NA
Length at birth	44 cm (5^{th})	53 cm (50-75^{th})		
Weight at birth	2.4 kg (25^{th})	3.3 kg (25-50^{th})		
Head circumference	34.8 cm (P75-90)	37 cm (90^{th})		
Stature at last evaluation	90^{th}	75-90^{th}	>P50 8/8	>P50 8/11
Weight at last evaluation	97^{th}	50-75^{th}	>P90 6/8	>P90 3/9
Head circumference at last evaluation	>97^{th}; +4.3SD	>97^{th}; +3.5SD		
Macrocephaly	+	+	+	+
Developmental delay	mild	+++	5+/3+++	11/12
Sitting age	11 months	19 months		
Walking age	18 months	24 months		
Cognitive impairment	reduced short-term memory	speech limited to few simple words		
IQ	77	NA		
Autism	-	-	4/8	3/12
Repetitive hand movements	-	++		
Abnormal brain imaging:				
prominent subarachnoid spaces	+	-		
hypoplastic corpus callosum	+	+ (partial agenesis)	8/8	4/7
small pituitary pars intermedia cyst	+	-		
Seizures/EEG anomalies	-	-	0/8	4/10
Muscular hypotonia	trunk	generalized	6/8	9/10
Distal muscle wasting	-	-	7/8	1/12
Joint contractures	+	-	5/7	0/4
Hip dysplasia	-	-	4/8	NA
Cryptorchidism	+ (treated 6y)	-	3/4	3/6
Hearing loss	-	bilateral	7/8	0/4
Strabismus	+ (left eye)	convergent	NA	NA

Disturbed glucose metabolism	NA	-	7/7	NA
Tumors	-	-	1/8	0/10
Minor anomalies:				
prominent occiput	+	-		
face and forehead	narrow	broad		
supraorbital ridges	underdeveloped	underdeveloped		
eyebrows	medial flaring and lateral thinning	medial flaring with lateral thinning		
palpebral fissures	narrow	short with deep-set eyes	7/8 deep-set eyes	4/9 deep-set eyes
downslanted palpebral fissures	+	+	7/8	6/12
malar flattening	+	+		
wide nasal bridge	+	+		
depressed nasal bridge	+	+		
broad nasal tip	+	short columella, thickened alae nasi		
philtrum	short and deep	deep		
upper and lower lip vermilion	thick and everted	thin upper lip vermilion, exaggerated cupid's bow, everted lower lip vermilion		
hypotonic mouth	+	slightly downturned angles		
teeth	delayed eruption	NA		
incisor diastema	mild	Mild		
Ears	Increased posterior angulation	long with increased posterior angulation	8/8 large	4/12 large
overfolded helices	+	-		
lobes	forward facing	-		
Hand	-	short broadened thumbs, short phalanx of the 5th, deep palmar creases		
Feet	-	bilateral sandal gaps		
Hair	-	initially full and curly, high anterior hairline, hypertrichosis of the back		

NA, not assessed

Stellacci, Steindl *et al.,* Clinical and functional characterization of two novel *ZBTB20* mutations causing Primrose syndrome.

SUPPORTING INFORMATION

SUPPLEMENTAL METHODS

Whole Exome Sequencing. Genomic DNA was extracted from leukocytes. Whole exome sequencing (WES) of patients and their parents was performed using the Agilent SureSelectXT Clinical Research Exome Kit (V5) with paired-end sequencing (HiSeq SBS Kit v4) on a HiSeq 2500 System (Illumina). Raw fastQ files were aligned to the hg19 reference genome using NextGene (Softgenetics). Variants observed in at least 16% of reads with sufficient quality level and minor allele frequency ≤ 2% were investigated *in silico* for deleterious effects using CADD. Potentially deleterious variants in genes functionally linked to developmental processes implicated in the patients' phenotype were further evaluated for compatibility with the expected mode of inheritance and for functionally annotated. Variant validation and segregation analyses were performed by Sanger sequencing using an ABI Genetic Analyzer 3730 (Applied Biosystems, USA).

Structural analysis. Structural analysis of the possible effects of the Thr644Ile substitution was performed using the VMD software (Humphrey et al, 1996), based on the homology model reported in Cordeddu *et al*. (2014).

Plasmid construction

The entire coding sequence of human wild-type *ZBTB20* was cloned in the pcDNA6/HisC and pFLAG-CMV vectors (*Kpn*I/*Xba*I sites) to generate an Xpress-tagged and a FLAG-tagged protein (tags at the *N*-terminus in both cases), respectively. The disease-causing c.1024delC (p.Gln342Serfs*42) and c.1931C>T (p.Thr644Ile) changes were introduced by using the QuikChange Site-Directed Mutagenesis Kit (Agilent Technologies, CA, USA).

Cell culture and DNA transfections. Human HEK293T kidney cells (from ATCC) were grown in Dulbecco Modified Eagle's Medium High Glucose (DMEM) containing 10% fetal bovine serum (FBS), supplemented with Penicillin, Streptomycin and L-Glutamine (all from Euroclone, Milan,

Italy). For transfection, polyethylenimine (PEI) reagent was obtained from Neo Transduction Laboratories (Lexington, KY, USA).

DNA affinity binding assays. For cell-based assays, HEK293T cells were transiently transfected with PEI, following the manufacturer's instructions. ZBTB20 expression data were obtained by western blot analysis from at least three independent experiments.
For DNA affinity binding assays, a biotinylated oligonucleotide corresponding to the *AFP* sequence containing the ZBTB20 specific DNA-binding site was synthesized (TTCAACCTAAGGAAATACCATAAAGTAACAGATATACCAACAAAAGGTTACTAGTT, forward strand). Processing of protein extracts from transfected cells and DNA affinity binding assays were performed as previously described (Fragale et al, 2011). Eluted material was separated onto 7.5% SDS-PAGE followed by immunoblotting with anti-Xpress monoclonal antibody (Invitrogen, Thermo Scientific, USA). Data were obtained from three independent experiments.

Confocal laser scanning microscopy. HEK293T cells were seeded on glass coverslips, maintained in culture in complete medium (24 h), and transiently transfected with Xpress-tagged *ZBTB20* mutant cDNAs and/or wild-type FLAG-tagged *ZBTB20*. Forty-eight hours post transfection, cells were treated with CSK buffer, fixed with 3% paraformaldehyde (30 min, 4 °C) and permeabilized with 0.5% Triton X-100 (10 min, room temperature). Cells were stained with anti-Xpress mouse monoclonal (1:100 dilution) and anti-FLAG rabbit monoclonal (1:100 dilution, SIGMA) antibodies, and Alexa Fluor-488 goat anti-mouse secondary antibody and Alexa Fluor-594 goat anti-rabbit (1:100 dilution, Molecular Probes, Thermo Scientific). After staining, coverslips were extensively rinsed and then mounted on the microscope slide by using Vectashield with DAPI mounting medium (Vector Laboratories). Observations were performed twice (>300 cells observed in each experiment) on a TCS SP2 AOBS apparatus (Leica Microsystems, Wetzlar, Germany), using 63X/1.4 NA oil objective and excitation spectral laser lines at 405 and 488 nm. Image acquisition and processing were performed by using the Leica Confocal Software (Leica Lasertechnik GmbH). Signals from different fluorescent probes were taken in sequential scanning mode.

REFERENCES

Schwede T, Kopp J, Guex N, Peitsch MC. SWISS-MODEL: An automated protein homology-modeling server. Nucleic Acids Res. 2003: 31:3381-3385.

Cordeddu V, Redeker B, Stellacci E, et al. 2014. Mutations in ZBTB20 cause Primrose syndrome. *Nat Genet* 46:815–817.

Humphrey W, Dalke A and Schulten K. VMD - Visual Molecular Dynamics. 1996. *J. Molec. Graphics*. Vol. 14, pp. 33-38.

Fragale A, Stellacci E, Ilari R, et al. Critical role of IRF-8 in negative regulation of TLR3 expression by Src homology 2 domain-containing protein tyrosine phosphatase-2 activity in human myeloid dendritic cells. 2011. *J Immunol.*186:1951-1962.

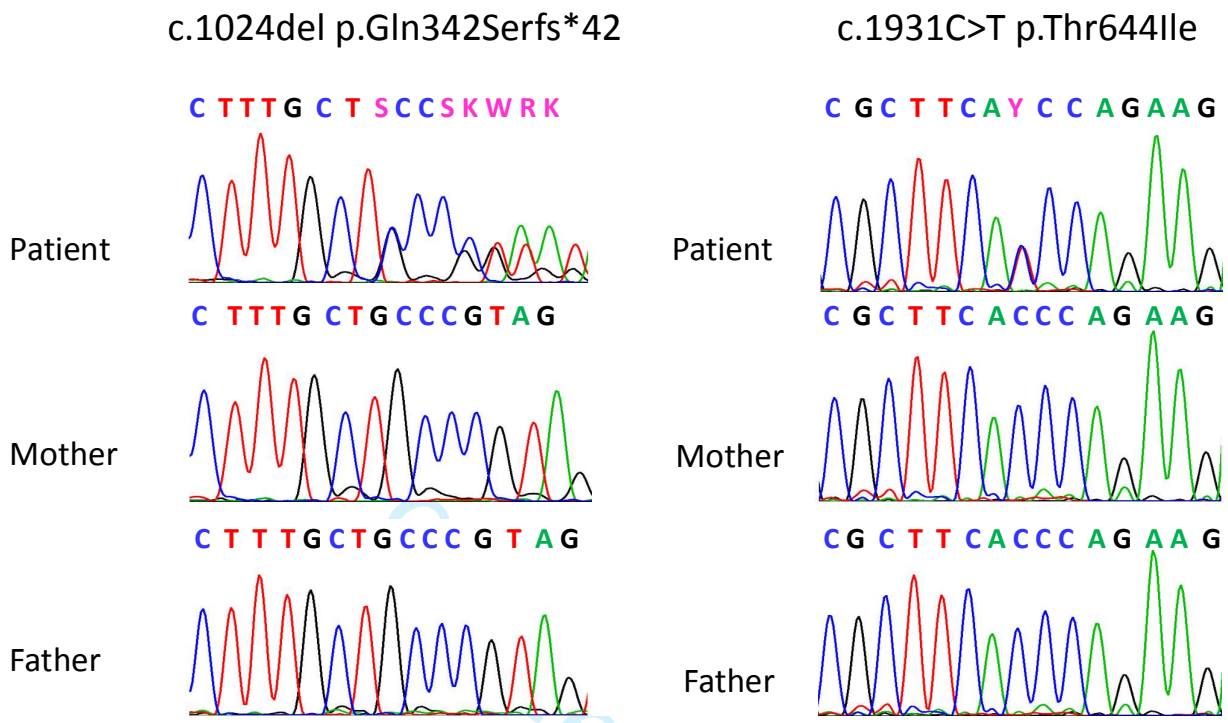

Supplementary Figure 1. Germline *ZBTB20* mutations causing Primrose syndrome. Sequence chromatograms showing the *de novo* origin of the identified *ZBTB20* missense changes in the two sporadic affected subjects, P1 (A) and P2 (B), included in the study.